Article

Immunity

Interleukin-12 and -23 Control Plasticity of CD127^{+} Group 1 and Group 3 Innate Lymphoid Cells in the Intestinal Lamina Propria

Graphical Abstract

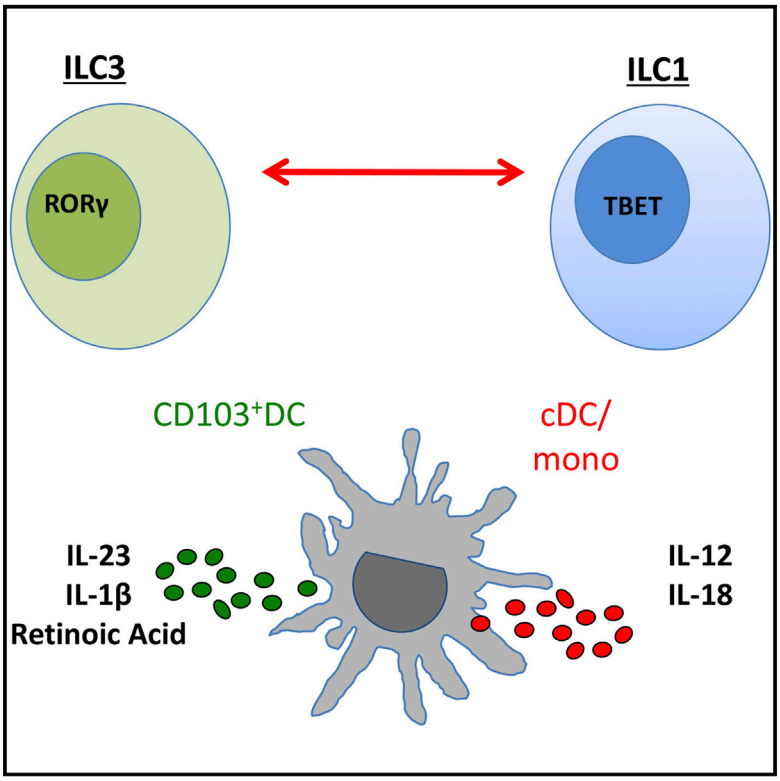

Authors

Jochem H. Bernink, Lisette Krabbendam, Kristine Germar, ..., Andreas Diefenbach, Bianca Blom, Hergen Spits

Correspondence

hergen.spits@amc.uva.nl

In Brief

Group 3 innate lymphoid cells (ILC3) can give rise to ILC1 in inflamed intestinal tissue. Spits and colleagues report bidirectional plasticity between ILC1 and ILC3 in the intestinal lamina propria in response to distinct environmental changes, suggesting functional adaptation without the need to recruit new cells from the circulation.

Highlights

- CD127^{+} ILC1 can differentiate into ILC3
- Differentiation of ILC1 to ILC3 is reversible
- Differentiation of ILC1 to ILC3 is driven by IL-23 and accelerated by IL-1β and RA
- Distinct dendritic cell subsets induce differentiation of ILC1 to ILC3 and vice versa

Bernink et al., 2015, Immunity *43*, 146–160
July 21, 2015
http://dx.doi.org/10.1016/j.immuni.2015.06.019

CellPress

CellPress

Immunity
Article

Interleukin-12 and -23 Control Plasticity of CD127$^+$ Group 1 and Group 3 Innate Lymphoid Cells in the Intestinal Lamina Propria

Jochem H. Bernink,[1] Lisette Krabbendam,[1] Kristine Germar,[1] Esther de Jong,[1] Konrad Gronke,[5] Michael Kofoed-Nielsen,[5] J. Marius Munneke,[2] Mette D. Hazenberg,[2] Julien Villaudy,[3] Christianne J. Buskens,[4] Willem A. Bemelman,[4] Andreas Diefenbach,[5] Bianca Blom,[1] and Hergen Spits[1,*]

[1]Department of Cell Biology and Histology
[2]Department of Hematology
[3]Department of Medical Microbiology
[4]Department of Surgery
Academic Medical Center, University of Amsterdam, Meibergdreef 9, 1105 AZ Amsterdam, the Netherlands
[5]Research Center Immunology and Institute of Medical Microbiology and Hygiene, University of Mainz Medical Centre, Obere Zahlbacher Strasse 67 D-55131 Mainz, Germany
*Correspondence: hergen.spits@amc.uva.nl
http://dx.doi.org/10.1016/j.immuni.2015.06.019

SUMMARY

Human group 1 ILCs consist of at least three phenotypically distinct subsets, including NK cells, CD127$^+$ ILC1, and intraepithelial CD103$^+$ ILC1. In inflamed intestinal tissues from Crohn's disease patients, numbers of CD127$^+$ ILC1 increased at the cost of ILC3. Here we found that differentiation of ILC3 to CD127$^+$ ILC1 is reversible in vitro and in vivo. CD127$^+$ ILC1 differentiated to ILC3 in the presence of interleukin-2 (IL-2), IL-23, and IL-1β dependent on the transcription factor RORγt, and this process was enhanced in the presence of retinoic acid. Furthermore, we observed in resection specimen from Crohn's disease patients a higher proportion of CD14$^+$ dendritic cells (DC), which in vitro promoted polarization from ILC3 to CD127$^+$ ILC1. In contrast, CD14$^-$ DCs promoted differentiation from CD127$^+$ ILC1 toward ILC3. These observations suggest that environmental cues determine the composition, function, and phenotype of CD127$^+$ ILC1 and ILC3 in the gut.

INTRODUCTION

The intestinal immune system is tolerant toward commensal bacteria but adroitly poised to fight invading pathogens. Homeostatic interactions between commensal bacteria and the intestinal immune cells contribute to the surveillance of the mucosal surface and maintenance of the epithelial barrier. Upon a pathogenic assault, the innate immune system responds promptly by tailoring an immune response accordingly to eliminate the pathogen or to instruct the adaptive arm of the immune system. Following the mounted immune response, a phase of resolution precedes the recovery of intestinal homeostasis and restoration of the intestinal architecture.

Innate lymphoid cells (ILCs) are a family of innate effector cells that are important not only for the integrity and maintenance of the intestinal tract but also in the protection against infiltrating pathogens at the acute phase of infection (Artis and Spits, 2015; Spits and Cupedo, 2012). Distinct ILC subsets respond to and protect against different pathogens by secreting cytokines that are similar to the cytokine and transcription factor expression pattern of the T helper cell family (Spits et al., 2012).

RORγt-expressing CD127$^+$ group 3 ILCs are involved in organizing tertiary lymphoid structures (van de Pavert and Mebius, 2010), are critical in controlling containment of commensals (Sonnenberg et al., 2012), and also promote antimicrobial peptide production and the proliferation of epithelial cells (Cella et al., 2009; Crellin et al., 2010). Furthermore, IL-22 producing group 3 ILCs protect against certain bacterial pathogens such as *Citrobacter rodentium*, which is used as a model in mice for the attaching and effacing *enteropathogenic Escherichia coli* (EPEC) and *enterohaemorrhagic E. coli* (EHEC) (Satoh-Takayama et al., 2008; Sonnenberg et al., 2011). T-bet-expressing group 1 ILCs protect against bacteria such as *Helicobacter typhlonius* (Powell et al., 2012) and intracellular pathogens such as *Salmonella enterica* in an IFN-γ-dependent manner (Klose et al., 2013).

Recently we identified a human ILC1 subset that like ILC2 and ILC3 expressed high amounts of the IL-7 receptor α-subunit (CD127) and the C-type lectin CD161. CD127$^+$ ILC1 lacked c-Kit and NKp44, which are expressed on all ILC3 and a subset of ILC3, respectively. Another group identified a distinct subset of group 1 ILCs, which were located in the intestinal epithelium (Fuchs et al., 2013). These ILC1 expressed the epithelial homing integrin CD103 and only low amounts of CD127. The relationship between these CD103$^+$ ILC1 and CD127$^+$ ILC1 is unclear. Here we compared the CD103$^+$ ILC1 and CD127$^+$ ILC1 in more detail.

Previously, we and others demonstrated that prolonged exposure to type 1 polarizing cytokines induced a change of ILC3 into c-Kit$^-$ NKp44$^-$ ILC1. This was accompanied by downregulating *RORC*, which was inversely proportional to the upregulation of

TBX21 and the production of IFN-γ (Bernink et al., 2013; Vonarbourg et al., 2010). In line with this observation, individuals with Crohn's disease—a typical type 1 inflammatory disease—displayed a reduced frequency of group 3 ILCs in inflamed ileal resection specimen, whereas group 1 ILCs were present in a considerably higher frequency compared to patients without intestinal inflammation (Bernink et al., 2013).

Here we addressed the question whether IFN-γ-producing group 1 ILCs have the potential to differentiate toward IL-22-producing ILC3. We demonstrated both in vitro and in vivo that human CD127$^+$ group 1—but not CD103$^+$ ILC1 or cNK cells—can differentiate into ILC3, depending on the cytokines they are exposed to, a process which is dependent on the transcription factor RORγt. Furthermore, we demonstrated that the gut metabolite retinoic acid (RA) accelerates transition of CD127$^+$ ILC1 to IL-22-producing ILC3, and we identified RA-producing CD103$^+$ dendritic cells (DCs) as a physiological source that could drive ILC differentiation and maintenance of ILC3.

RESULTS

CD127 and CD103 Define Distinct ILC1 Subsets

Human group 1 ILCs comprise a heterogeneous population of IFN-γ-producing effector cells, including conventional natural killer (cNK) cells and two populations of ILC1. The first ILC1 subset described by our group (Bernink et al., 2013) expresses high amount of CD127 (the IL-7Rα chain), and is referred to as CD127$^+$ ILC1. The ILC1 subset described by Fuchs et al. (2013) expresses CD103 (an intergrin αE subunit), which in association with β7 may play a role in homing of intraepithelial lymphocytes. This ILC1 subset is therefore referred to as CD103$^+$ ILC1. In order to obtain more insight into the functional differences between CD127$^+$ and CD103$^+$ ILC1, we first compared the phenotype and tissue distribution of the two ILC1 subsets in human palatine tonsils, ileum, and mesenteric lymph node. CD103$^+$ ILC1, which could be distinguished from CD127$^+$ ILC1 by the expression of CD56, NKp44, and CD103 were detected in tonsil and ileum, but not in mesenteric lymph node (Figure 1A). The frequencies of CD127$^+$ and CD103$^+$ ILC1 subsets in tonsils were similar, but were less compared to NKp44$^+$ and NKp44$^-$ ILC3 (Figure 1A). In the ileum, the CD103$^+$ ILC1 were found in the epithelium as documented before (Fuchs et al., 2013), whereas the CD127$^+$ ILC1 were present in the lamina propria (Figure 1A). Compared to CD127$^+$ ILC1, CD103$^+$ ILC1 expressed very little CD127 if at all (Figure 1B). CD103$^+$ ILC1 from tonsils expressed CD94 and are heterogeneous for CD160, whereas CD127$^+$ ILC1 were negative for both markers (Figure 1B). Both ILC1 subsets expressed CD161, but CD103$^+$ ILC1 showed much lower expression compared to CD127$^+$ ILC1 (Figure 1B). Like CD103$^+$ ILC1, conventional cNK cells expressed CD56 and CD94 and were heterogeneous for CD160, but lacked expression of CD103, and CD161 (Figure 1B).

We next analyzed the expression of transcription factors in freshly isolated ILC subsets. Transcripts of the transcription factor RORγt (*RORC*) were undetectable in ex vivo isolated CD103$^+$ ILC1, and low—but not absent—in CD127$^+$ ILC1 compared to NKp44$^-$ and NKp44$^+$ ILC3 subsets (Figure 1C). *TBX21*, which encodes for the transcription factor T-bet was expressed at highest levels in CD103$^+$ ILC1 and CD127$^+$ ILC1 as compared to both ILC3 subsets. The transcription factor Eomesodermin (Eomes), which has been associated with cNK cells in mice (Daussy et al., 2014; Gordon et al., 2012; Klose et al., 2014), was highly expressed in CD103$^+$ ILC1, but absent in all CD127$^+$ ILC1 and ILC3 subsets (Figure 1C). As expected, both ILC1 subsets but not ILC3, expressed transcripts for *IFNG*, which was most pronounced in CD103$^+$ ILC1. *IL22* transcripts were highly expressed in the NKp44$^+$ ILC3 subset. The transcription factor arylhydrocarbon receptor (*AHR*) was expressed in all ILC subsets, but highest in ILC3. Freshly isolated intestinal ILC subsets showed a similar transcription factor expression profile compared to their tonsil counterparts (Figure S1A).

In contrast to ex vivo isolated cNK cells, CD103$^+$ and CD127$^+$ ILC1 did not produce IFN-γ in response to IL-15 alone as measured by enzyme-linked immunosorbent assay (ELISA) (Figure 1D). Combined stimulation with IL-15 and IL-12 resulted in a robust IFN-γ response in all ILC1 subsets, which was most pronounced in cNK cells. Stimulation with the pro-inflammatory cytokines IL-12 plus IL-18 induced a similar response in all group 1 ILC subsets and was higher compared to stimulation with IL-12 plus IL-15.

Together, these data demonstrate that in addition to cNK cells, two distinct human IFN-γ producing group 1 ILC subsets are present in the tonsil and ileum, which have the ability to respond to the pro-inflammatory cytokines IL-12, IL-15, and IL-18 ex vivo.

When comparing the ILC composition of fetal intestine to that of non-inflamed and inflamed resection specimens from patients that suffer from Crohn's disease, we observed that CD127$^+$ ILC1 in fetal intestines, which were not yet colonized with commensal bacteria, were very low in frequency, and we did not observe any CD103$^+$ ILCs (Figure 1E; Figure S1B). Furthermore, we observed that fetal intestinal NKp44$^-$ ILC3 expressed CD103, whereas this marker was restricted to CD103$^+$ ILC1 in adult gut and tonsils (Figure S1C). The frequency of CRTH2$^+$ group 2 ILCs in the fetal intestines decreased in post-natal intestinal tissues. Furthermore, whereas in adult non-inflamed intestinal resection specimen the frequencies of CD103$^+$ ILC1 and CD127$^+$ ILC1 were the same, lamina propria CD127$^+$ ILC1 expanded dramatically in inflamed ileum resected from Crohn's disease patients, outnumbering intraepithelial CD103$^+$ ILC1, which expanded less than 2-fold (Figure 1E; Figure S1D). No significant changes in frequency were observed for cNK cells between non-inflamed and inflamed Crohn's ileum (Figure S1E).

Together, these data confirm that CD103$^+$ ILC1 are restricted to the intraepithelial compartment (Fuchs et al., 2013), whereas CD127$^+$ ILC1 are found within the lamina propria. Furthermore, CD127$^+$ ILC1 outnumbered CD103$^+$ ILC1 in inflamed gut tissues of Crohn's disease patients.

IL-23 and IL-1β Are Sufficient to Drive Differentiation of CD127$^+$ ILC1 toward ILC3

Differentiation of ILC3 toward IFN-γ-producing CD127$^+$ ILC1 under influence of IL-12 may contribute to the increase in frequency of CD127$^+$ ILC1 in inflamed mucosal tissues as seen in the inflamed intestines of individuals with Crohn's disease (Bernink et al., 2013; Vonarbourg et al., 2010). We then asked whether IFN-γ-producing ILC1 have also the potential to differentiate toward IL-22 producing ILC3. To address this question, we sorted

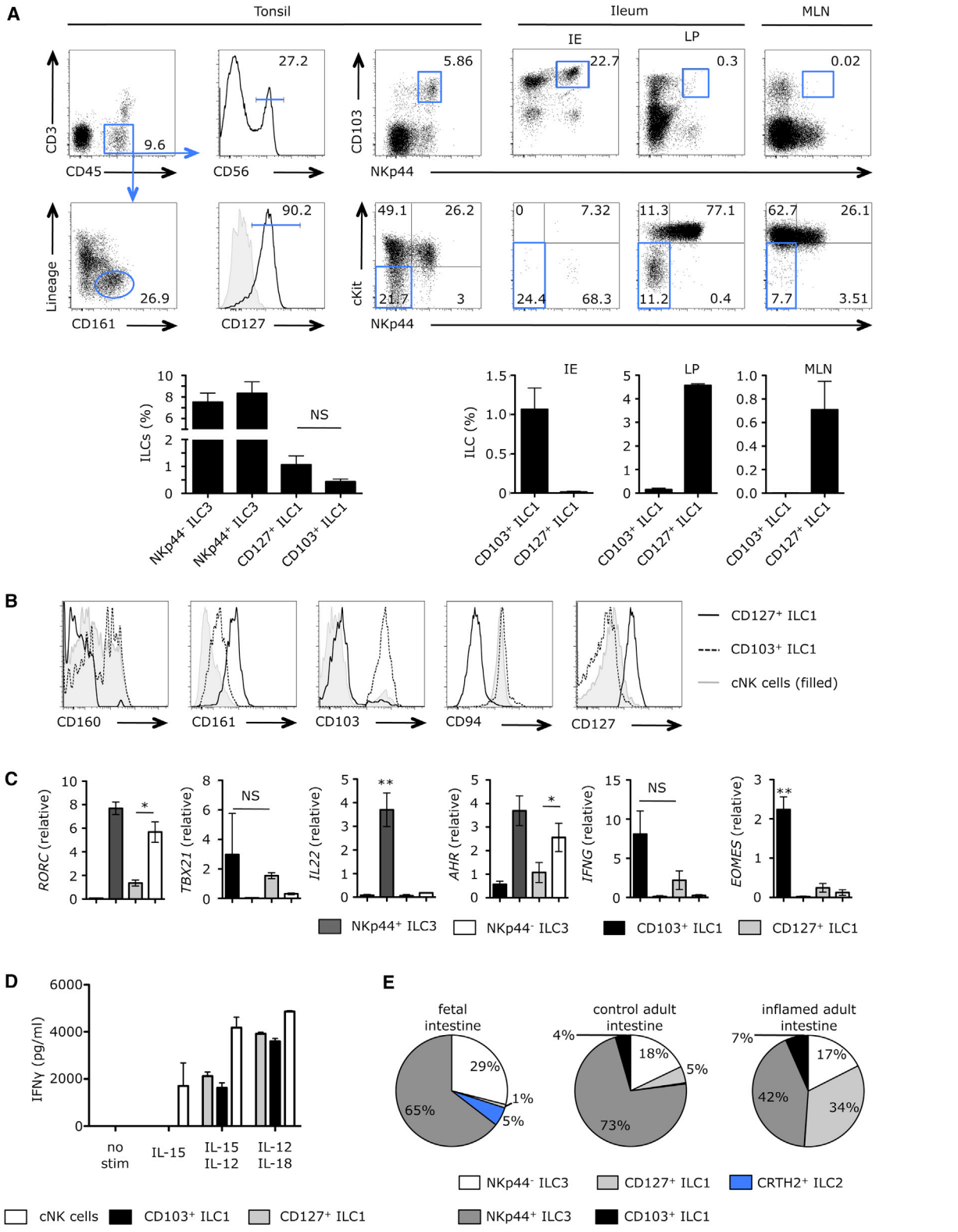

Figure 1. Phenotype, Function, and Distribution of CD127⁺ and CD103⁺ ILC1 in Human Tonsil, Intestine, and Mesenteric Lymph Node

(A) Flow cytometric analysis of the expression of CD103⁺ ILC1 and CD127⁺ ILC1 in freshly isolated tonsil mononuclear cells, which are depleted from T cells (CD3) and B cells (CD19) by magnetic bead-based separation, in freshly isolated intestinal epithelial cell (IE) and lamina propria (LP) fraction of resection specimen, and freshly mesenteric lymph nodes (MLN). Subsets were gated on CD3⁻ and CD45⁺ followed by gating on either CD56, CD103, and NKp44 for CD103⁺ ILC1, or

(legend continued on next page)

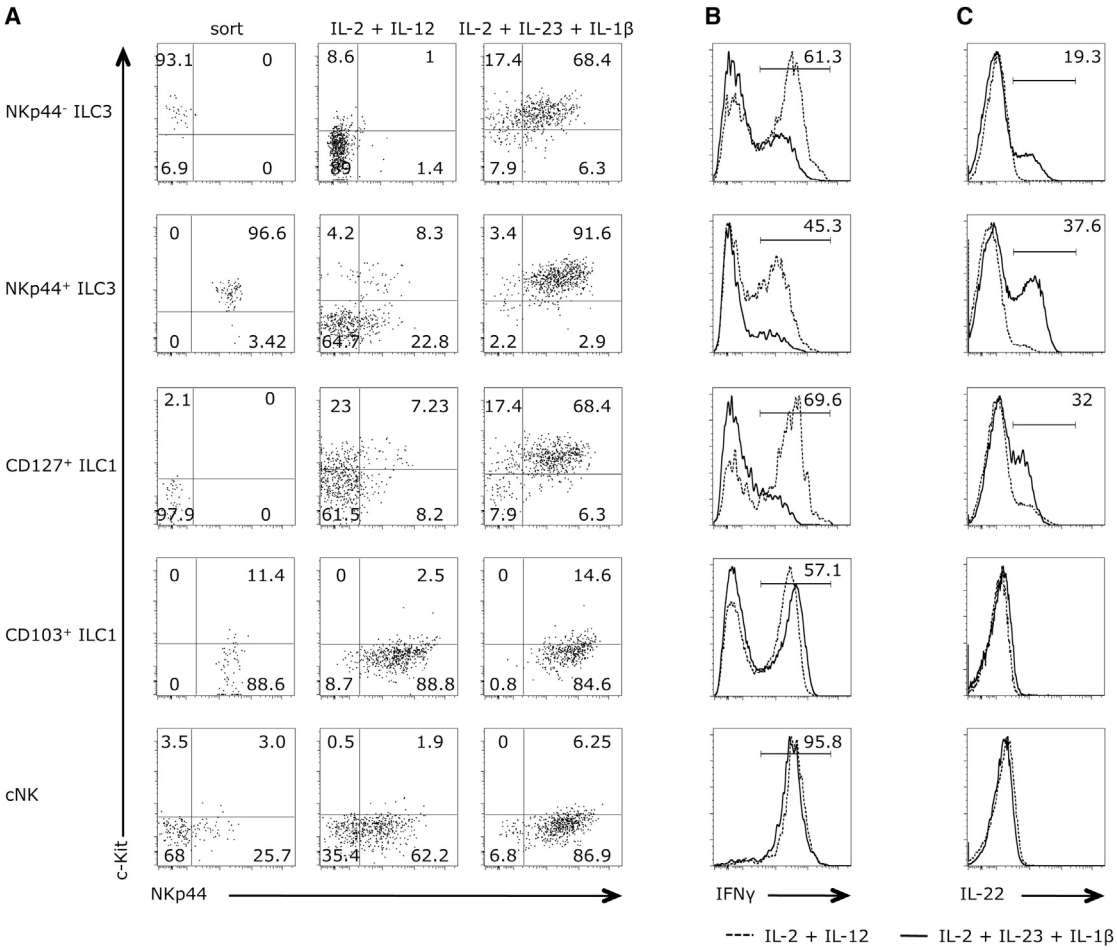

Figure 2. IL-2, IL-23, and IL-1β Drive ILC3 Differentiation

(A) Purified CD127$^+$ ILC1, NKp44$^-$ ILC3, NKp44$^+$ ILC3, CD103$^+$ ILC1, and cNK cells from tonsil were cultured for 4 days either with IL-2 and IL-12 or with IL-2, IL-23, and IL-1β. Cells were phenotyped for the expression of c-Kit and NKp44. Numbers in quadrants indicate percent cells in each. Data shown is representative of 4 experiments.

(B) Expression of intracellular IFN-γ measured by flow cytometry of either IL-2 and IL-12 (dashed line) or IL-2, IL-1b, and IL-23 (black line) cultured subsets in (A), following stimulation with PMA plus ionomycin. Data shown is representative of 3 experiments.

(C) Expression of intracellular IL-22 measured by flow cytometry of either IL-2 and IL-12 (dashed line) or IL-2, IL-1b, and IL-23 (black line) cultured subsets in (A), following stimulation with PMA plus ionomycin. Data shown is representative of 3 experiments.

CD127$^+$ ILC1, NKp44$^-$ ILC3, NKp44$^+$ ILC3, CD103$^+$ ILC1, and cNK cells (Figure 2A, left column), and cultured these cells for 4 days in the presence of feeder cells with IL-2 and IL-12, or IL-23, and IL-1β. As documented previously (Bernink et al., 2013; Cella et al., 2010), IL-2, IL-23, and IL-1β maintained the ILC3 phenotype, and promoted the acquisition of NKp44. Furthermore, IL-2 and IL-12 was sufficient to induce differentiation of NKp44$^-$ and NKp44$^+$ ILC3 toward CD127$^+$ ILC1 (Bernink

selecting for Lin$^-$ (CD1a$^-$ CD3$^-$ CD14$^-$ CD19$^-$ CD94$^-$ CD34$^-$ CD123$^-$ TCRαβ$^-$ TCRγδ$^-$ BDCA2$^-$ FcεR1$^-$; Table S1), CRTH2$^-$ and CD161$^+$, CD127$^+$, and NKp44$^-$ and c-Kit$^-$ for CD127$^+$ ILC1, both indicated in blue box. Numbers in gates (outlined areas) or quadrants indicate percent cells in each. Distribution of ILC1 subsets in tissues is quantified in bar diagrams as percentage (%) of the total CD45$^+$ CD3$^-$ lymphocyte population. Data shown for tonsil is representative of at least 15 experiments, with one to two donors each, and intestinal data is representative of at least 6 experiments, one donor each.

(B) Flow cytometric analysis of CD127$^+$ ILC1 (black line), CD103$^+$ ILC1 (dashed line), and cNK cells (gray filled) of indicated surface molecules. Gating strategy used is as in Figure 1A. Data shown is representative of at least 4 experiments.

(C) Expression of *RORC*, *TBX21*, *IL22*, *AHR*, *IFNG*, and *EOMES* in the CD127$^+$ ILC1, NKp44$^-$ ILC3, NKp44$^+$ ILC3, and CD103$^+$ ILC subsets of freshly isolated tonsils, presented relative to the expression of *ACTB* (which encodes β-actin). Data shown is combined data of at least 3 experiments, each with 1 to 2 donors each.

(D) IFN-γ-production by CD127$^+$ ILC1 (black), and CD103$^+$ ILC1 (white), and cNK cells (gray), cultured for 4 days, either alone or IL-15 and/or IL-12, and IL-12 with IL-18.

(E) Mean frequency (as percentage of total ILCs per sample) of CD103$^+$ ILC1, CD127$^+$ ILC1, CRTH2$^+$ ILC2, NKp44$^-$ ILC3, and NKp44$^+$ ILC3 within fetal intestine (N = 12), non-inflamed control intestine (N = 6), and Crohn's disease intestine (N = 6). In these experiments IE and LP fractions were combined before analysis. *$p < 0.05$, **$p < 0.01$ (ANOVA). Error bars (A, C, D) represent SEM.

et al., 2013), and CD127$^+$ ILC1 cultured in the presence of IL-2 and IL-12 maintained their phenotype (Figure 2A). Although CD127$^+$ ILC1 showed only a modest expression of IL-1R and IL-23R compared to ILC3 (Figure S2), CD127$^+$ ILC1 differentiated toward ILC3 when cultured with IL-1β, IL-2, and IL-23 (Figure 2A). As a consequence, CD127$^+$ ILC1 lost their potential to produce large amounts of IFN-γ, and instead started to produce IL-22 (Figures 2B and 2C). Neither CD103$^+$ ILC1 nor cNK cells differentiated into ILC3 or produced IL-22 (Figures 2A–2C).

IL-22 and IL-17 production is restricted to lymphocytes that express the transcription factor RORγt (Ivanov et al., 2006), whereas IFN-γ production is associated with high expression of the transcription factor T-bet (Lazarevic et al., 2011). Given the plasticity of the CD127$^+$ ILC subsets in their cytokine expression pattern, we asked whether the transcription factor program adapted accordingly. As such, we purified ILC subsets from tonsils and intestinal resection specimens and cultured these cells for 4 days in the presence of feeder cells with IL-2 and IL-12, or IL-2 IL-23 and IL-1β (Figures S3A–S3F). Indeed, NKp44$^+$ ILC3 lost their RORγt expression upon exposure to IL-2 and IL-12, whereas T-bet was upregulated (Figures S3A and S3B). Also, we observed a change into an ILC3-like transcription factor profile in CD127$^+$ ILC1 when exposed to IL-2, IL-23, and IL-1β (Figures S3A and S3B). Notably, neither in ILC3 nor in CD127$^+$ ILC1 we observed Eomes (Figure S3C). This was in sharp contrast to cNK cells and CD103$^+$ ILC1, which did not express RORγt, but rather maintained or enhanced their expression of T-bet and Eomes (Figures S3C and S3F).

The observation that CD127$^+$ ILC1 acquire phenotypic and functional features of ILC3 may be the result of outgrowth of a small number of ILC3 contaminating the purified ILC1. In that case, the ILC3 should have undergone many cell divisions. To address this, we labeled sorted CD127$^+$ ILC1 with a cell tracer dye and cultured them in the presence of IL-2, IL-23, and IL-1β. Electronic gating on cells that expressed high amounts of the cell tracer, and thus did not proliferate, revealed that these cells expressed c-Kit and NKp44, indicating that the non-proliferated fraction of CD127$^+$ ILC1 differentiated toward ILC3 (Figure 3A). This observation argues against the possibility that outgrowth of contaminating ILC3 in CD127$^+$ ILC1 cultures accounted for the observed phenotype. Furthermore, we did not detect any difference in viability between the non- and proliferating cell fractions (Figure 3B). Further supporting our hypothesis, we sorted out ILC3-derived ILC1 and observed that these cells could re-differentiate toward ILC3 in the in the presence of IL2, IL-23, and IL-1β (Figure S4).

To further confirm that the CD127$^+$ ILC1 can differentiate to ILC3, we generated clones of purified ILC1 (>97%) in the presence of feeder cells and IL-2, IL-1β, and IL-23. No difference was observed in the plating efficiencies between the two ILC3 populations and ILC1 under these conditions (Figure 3C). The burst size after 14 days of culture was on the average 4,000 cells per well (Figure 3D), allowing for a phenotypic evaluation of the progeny of the individual ILC1. Most ILC1-derived clones showed a heterogeneous phenotype as exemplified in the left panel of Figure 3E; the right panel shows an overview of the distribution of nine individual clones within the progeny of one single cell. We observed cells with a phenotype of ILC1, NKp44$^-$ ILC3, and NKp44$^+$ ILC3 (Figure 3E). In addition, we observed clones that were partly NKp44$^+$ c-Kit$^-$. Cells with a similar phenotype were also observed in ex vivo isolated ILCs (Bernink et al., 2013) and have yet to be characterized in more detail. The different phenotypes we observed within a clone correlated with different functional capacities, because c-Kit$^+$ cells isolated from the progeny of a single ILC1 produced mainly IL-22 and little IFN-γ, whereas c-Kit$^-$ NKp44$^-$ cells isolated from the same cell samples produced IFN-γ and little IL-22 (Figure 3F). These data support the notion that a sizeable fraction of CD127$^+$ ILC1 can differentiate into IL-22 producing ILC3 in the presence of the cytokines IL-2, IL-23, and IL-1β.

ILC1 Differentiate toward ILC3 In Vivo

Previously, we demonstrated that CD127$^+$ ILC1 accumulated at the onset of intestinal inflammation in mice that were reconstituted with a human immune system (HIS) (Bernink et al., 2013). In order to evaluate whether the observed ILC1 to ILC3 differentiation in vitro also occurred in humanized mice without inflammation, we engrafted sub-lethally irradiated lymphopenic mice (NOD SCID *IL2GC*$^{-/-}$; NSG) with human hematopoietic stem cells (HIS-mice). First we analyzed the ILC1 and ILC3 composition in blood, spleen, lung, small intestine, and colon, which were reconstituted on average up to 80% with human cells at the age of 8 weeks (Figures 4A and 4B; Figure S5A). Next, we injected humanized mice intravenously (i.v.) with expanded ILC1 as described previously (Bernink et al., 2013), which were labeled with a cell tracer dye (Figure S5B). This allowed us to trace the fate of ILC1 in vivo under homeostatic conditions. Analyses of blood, spleen, liver, lung, small intestine and colon revealed that cell tracker-positive ILCs were clearly detectable in all organs 4 days after injection (Figure 4C; Figure S5B). Interestingly, the ILC distribution-profile of cell tracer-positive ILCs is similar to the human ILC profile derived from the injected hematopoietic stem cells (Figure 4B), which was particularly emphasized in the small intestine, as also NKp44$^+$ ILC3 were detectable (Figure 4D).

ILCs in mice and humans are very similar in functional respects although phenotypic differences are obvious. It has been documented also in mouse that ILC3 can lose RORγt and upregulate T-bet and their capacity to produce IFN-γ (Cella et al., 2010; Vonarbourg et al., 2010). Based on our findings, we expected that these murine ILC3-derived ILC1 (also called ex-RORγt$^+$ ILC3) can differentiate back to ILC3 under homeostatic conditions. To examine this, we reconstituted lymphopenic mice (*Rag2*$^{-/-}$ *Il2rg*$^{-/-}$) with murine NKp46$^+$ NK1.1$^+$ RORγt-fate-map (fm)$^+$ ILC3, which had downregulated RORγt expression (ex-RORγt$^+$ ILC3) (Klose et al., 2013) (Figure S5C). Analysis of small and large intestine 6 weeks after injection revealed that, ILC3-derived ILC1 upregulated RORγt expression (Figure 4E). Together, these data indicate that in the absence of inflammation, CD127$^+$ ILC1 can switch toward ILC3 in vivo.

Retinoic Acid Accelerates ILC3 Differentiation and IL-22 Production

The vitamin A metabolite retinoic acid (RA) has recently been reported to enhance IL-22 production by ILC3 in mice (Mielke et al., 2013). Here we investigated whether RA contributes to the differentiation of ILC1 toward ILC3. The subunits for the receptor for RA, retinoic acid receptor α (*RARA*), γ (*RARG*), and *RXRG* were

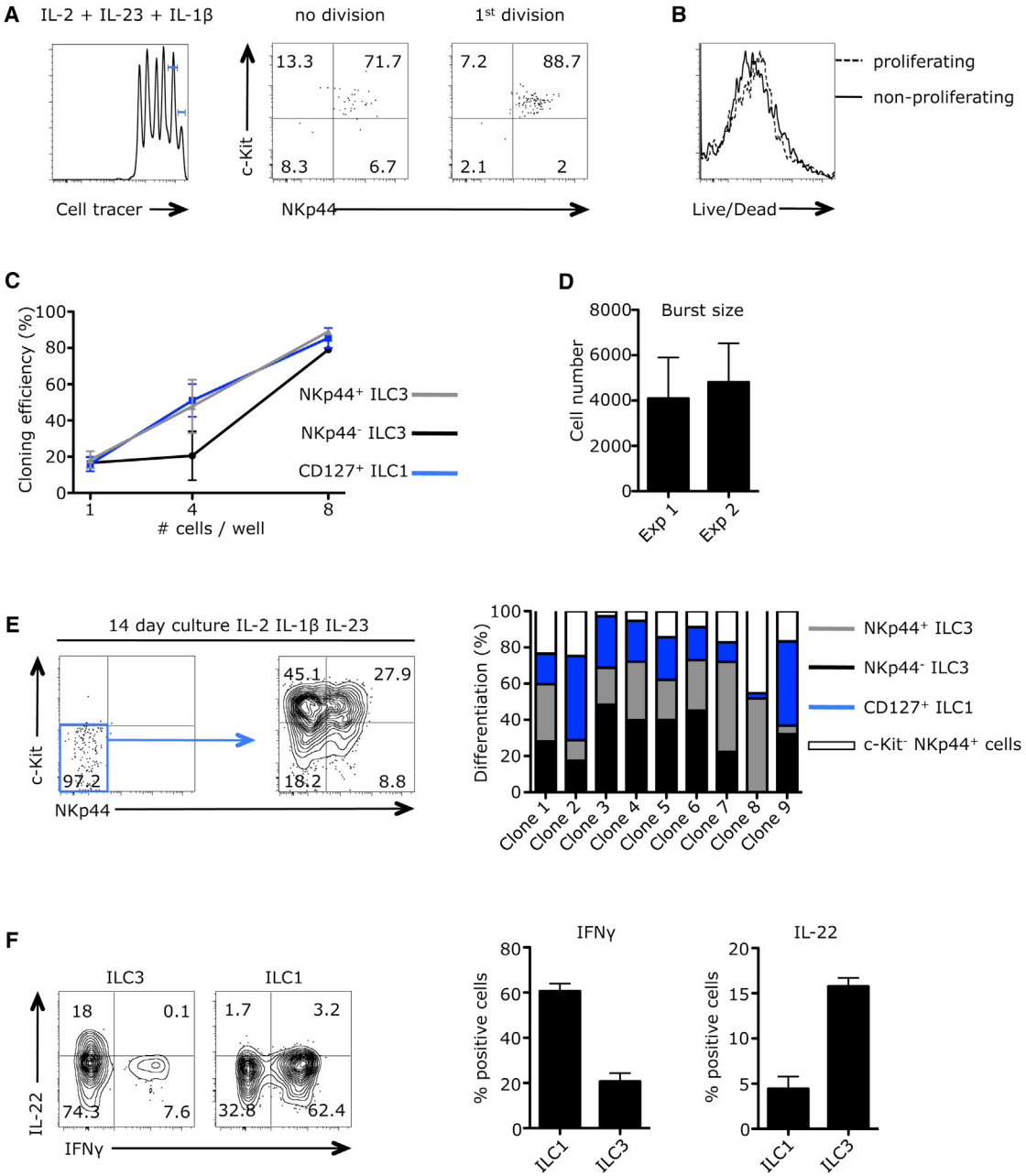

Figure 3. CD127⁺ ILC1 Clones Give Rise to IL-22 Producing ILC3 Subsets

(A) Flow cytometry of purified CD127⁺ ILC1 from tonsil, stimulated for 7 days with IL-2 IL-23 IL-1β, and stained with a proliferation dye. Numbers above bracketed lines indicate percent of non-dividing cells and after first division, followed by phenotyping for the expression of c-Kit and NKp44. Numbers in quadrants indicate percentage cells in each. Data shown is representative of 3 experiments.

(B) CD127⁺ ILC1 sorted from tonsil have been cultured for 5 days with IL-2, IL-23, and IL-1β. Non-proliferating cells (dashed line) and proliferating cells (black line) were stained with a live/dead marker.

(C) Cloning efficiency of CD127⁺ ILC1, NKp44⁻ ILC3, and NKp44⁺ ILC3 was tested in cultures with 1, 4, and 8 cells per well with IL-2, IL-23, and IL-1β, and feeder cells for 14 days.

(D–F) Clonal burst sizes of two independent experiments were calculated based on the cloning efficiency assay. (E) Phenotyping and quantification of the expression of c-Kit and NKp44 in expanded CD127⁺ ILC1 clones. (F) IL-22 and IFN-γ production of clone 3, 4, and 5 derived ILC1 and ILC3 fractions. Error bars (C, D, F) represent SEM.

readily detectable in freshly isolated CD127⁺ ILC subsets (Figure 5A), suggesting that these cells are responsive to RA. Purified NKp44⁻ ILC3 and CD127⁺ ILC1 stimulated with the combination with IL-2, IL-1β, and IL-23 upregulated NKp44, and this effect was further enhanced by the addition of RA (Figure 5B), suggesting that RA accelerated differentiation. In line with these results,

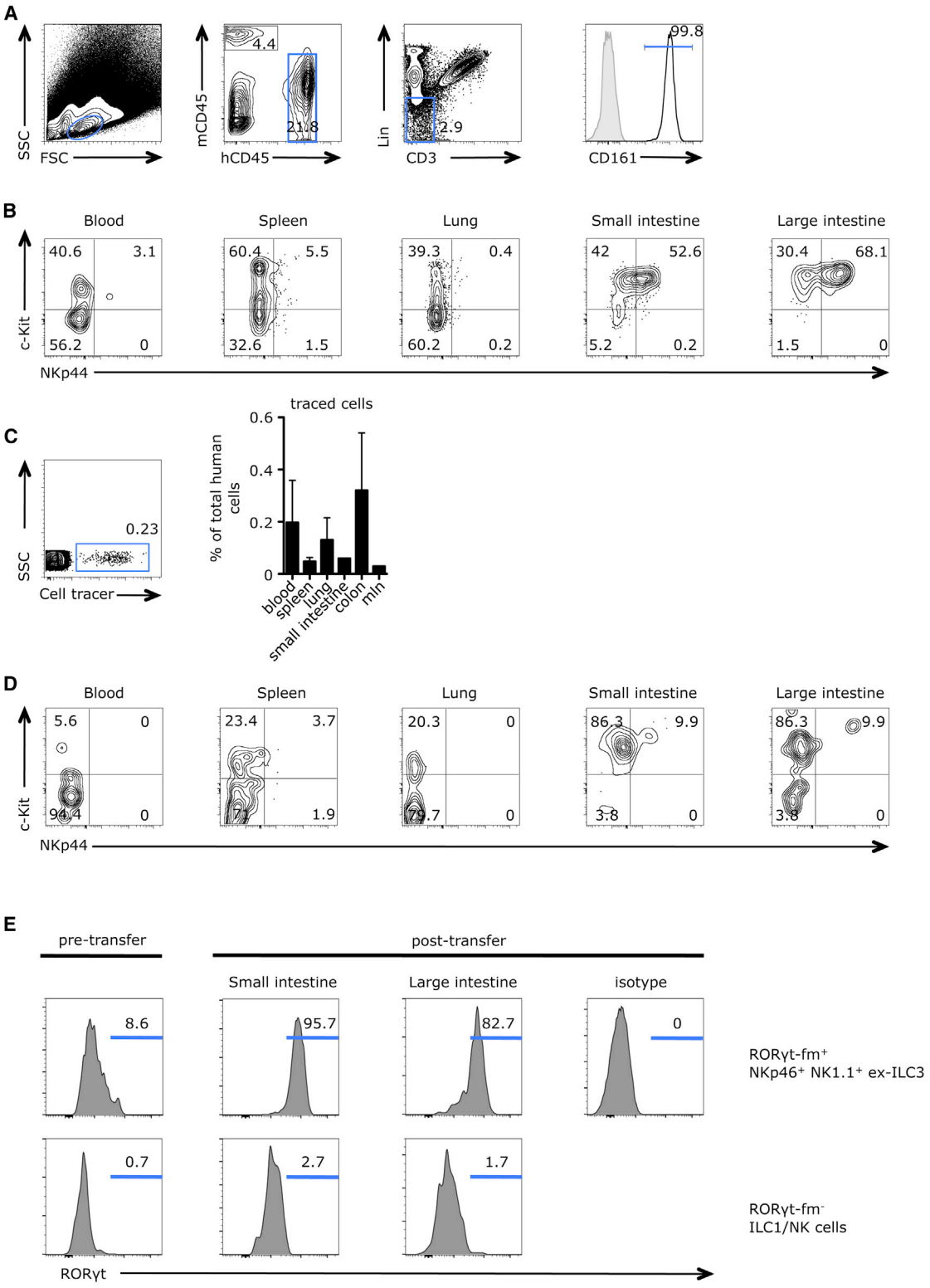

Figure 4. Expanded ILC1 Differentiate to ILC3 in NOD SCID *IL2gc*$^{-/-}$ (NSG) Mice that Were Engrafted with Human Immune Cells

(A) Gating strategy of human ILCs of the lamina propria mononuclear cells fraction of the large intestine in humanized mice. Cells were electronically gated on lymphoid cells, followed by gating on human (h) CD45 cells. Then gating strategy was used as in Figure 1A.

(B) Using gating strategy as in Figure 4A, blood, spleen, lung, small intestine, and large intestine were analyzed for the expression of c-Kit and NKp44.

(legend continued on next page)

we observed that RA enhanced upregulation of RORγt in CD127$^+$ ILC1 cultured with IL-2, IL-23, and IL-1β as compared to IL-2 alone (Figure 5C).

Next, we measured IL-22 protein by ELISA in cultures that started with purified CD127$^+$ ILC1. Culture with RA alone did not result in any production of IL-22. However, when cultured for 7 days in combination with IL-2, IL-23, and IL-1β, increased amounts of IL-22 were found in the culture supernatants of CD127$^+$ ILC1, and further increased in the presence of RA (Figure 5D), indicating that following differentiation of ILC1 to NKp44$^+$ ILC3, these cells started to produce IL-22. RA did not induce a notable production of IL-22 in either CD103$^+$ ILC1 or cNK cells (Figure S6). Cells cultured in the presence of RA showed a reduced proliferating capacity (Figure 5E). Thus, although RA enhanced differentiation of ILC1 into functional ILC3, it also reduced expansion of the ILC3 pool.

Differentiation of CD127$^+$ ILC1 to ILC3 Is Controlled by RORγt

Given the plasticity among the CD127$^+$ ILCs in terms of transcription factor and cytokine expression profile, we asked whether differentiation of CD127$^+$ ILC1 to ILC3 was controlled by the transcription factor RORγt. To address this question, we cultured purified tonsil CD127$^+$ ILC1 and ILC3 for 4 days with IL-2, IL-23, and IL-1β in the presence or absence of SR1001, a synthetic RORγt ligand, which induces suppression of the receptor's transcriptional activity (Solt et al., 2011). SR1001 inhibited differentiation of CD127$^+$ ILC1 to ILC3 compared to the DMSO control, as reflected by their hampered upregulation of c-Kit and NKp44 and reduced IL-22 production, whereas the cell number did not differ (Figures 6A and 6B). SR1001 variably affected IL-22 production by NKp44$^-$ ILC3, compared to the DMSO control as measured by ELISA (Figure 6B), but SR1001 did not substantially affect the ability of ex vivo isolated NKp44$^+$ ILC3 to produce IL-22.

Together, these data indicate that RORγt is important for the differentiation from CD127$^+$ ILC1 toward IL-22 producing ILC3 but may not be involved in IL-22 production after completion of the differentiation process.

ILC Plasticity Is Instructed by Dendritic Cells

The finding that CD127$^+$ ILC1 can differentiate into ILC3 raises the question which cell type may induce this differentiation. We examined the frequencies of HLA-DR$^+$ CD11c$^+$ dendritic cells (DCs) in Crohn's ileum compared to non-inflamed control. We observed that a significantly greater proportion of DCs in the inflamed gut expressed CD14 and that the CD14 expression levels were higher than on CD14$^+$ DC from non-inflamed tissue (Figure 7A). While there was no detectable difference in the expression of *IL23A* between CD14$^-$ and CD14$^+$ DCs, the latter did show increased expression of *IL12A* (Figure 7B), indicating a potential role for these cells in the differentiation into CD127$^+$ ILC1. In order to investigate the differential potential of these two DC subsets in promoting and maintaining the ILC1 phenotype, we cultured CD127$^+$ ILC1 or NKp44$^+$ ILC3 in the presence of autologous CD14$^+$ or CD14$^-$ DCs. CD127$^+$ ILC1 maintained their phenotype when cultured with CD14$^+$ DCs but upregulated c-Kit and NKp44 to adopt an ILC3 phenotype when cultured with CD14$^-$ DCs. In contrast, NKp44$^+$ ILC3 differentiated to the CD127$^+$ ILC1 phenotype in the presence of CD14$^+$ DCs but maintained their signature c-Kit and NKp44 expression when cultured with CD14$^-$ DCs (Figure 7C). Similar results were also obtained in an allogeneic setting in which fetal intestinal DCs were co-cultured with freshly isolated tonsillar ILCs. In these experiments, lipopolysaccharide (LPS) activated CD14$^+$ DCs promoted differentiation of NKp44$^+$ ILC3 to CD127$^+$ ILC1, whereas CD14$^-$ DCs favored development of ILC3 (Figure S7A). In contrast to intestinal CD14$^+$ DCs, CD14$^-$ DCs are heterogeneous in their expression of CD103 (Figure 7D). As CD103$^+$ DCs have been demonstrated to produce RA (Coombes et al., 2007; Sanders et al., 2014), we asked whether CD103$^+$ DCs are sufficient to drive ILC3 conversion. To this end, we employed a recently described in vitro monocyte derived DC (mDC) culturing system (Bakdash et al., 2014). We cultured peripheral blood derived CD14$^+$ monocytes in the presence of GM-CSF and IL-4 in the presence or absence of RA. Only mDCs cultured in the presence of RA (RA-mDC) upregulated CD103 and started to produce RA both under basal conditions (Bakdash et al., 2014), as well as upon stimulation with LPS as measured by the activity of the enzyme aldehyde dehydrogenase (ALDH), which drives the conversion of retinaldehyde into RA (Figure S7B). As a control we used diethylaminobenzaldehyde (DEAB), which inhibited ALDH activity, and thereby the conversion of retinol to RA. RA-mDC also expressed higher levels of *IL23A* transcripts upon LPS or polyI:C stimulation as compared to mDC (Figure S7C). In contrast, mDC expressed higher *IL12A* transcripts upon stimulation with either poly I:C or LPS compared to RA-mDC (Figure S7C). In line with these findings we observed that CD127$^+$ ILC1 cultures with activated RA-mDC induced an enhanced differentiation toward ILC3 compared to mDCs (Figure 7E). Together these in vitro experiments show that ILC3 have the capacity to differentiate into CD127$^+$ ILC1 and vice versa, depending on the milieu they are exposed to.

DISCUSSION

Group 2 and group 3 ILC subsets have been well characterized, whereas group 1 ILCs are less clearly defined. Recently, we and

(C) Humanized mice were retro-orbitally inoculated with expanded and with cell tracker labeled ILC1 (~$1 \times 10^5 - 5 \times 10^5$ cells per mouse) 4 days before analysis. Percentage of cell tracker positive ILCs compared to total hCD45 ILCs in analyzed organs varied between 0% and 0.5%. Left, large intestine; right, bar diagram indicating percentage of cell tracker positive ILCs per organ.

(D) Using gating strategy as in Figures 4A and 4C, blood, spleen, lung, small intestine, and large intestine were analyzed for the expression of c-Kit and NKp44. Data shown is representative of 3 experiments, each with 2 humanized mice (1–3 donors each), and reconstituted cells are from 1 donor each.

(E) Ex-RORγt$^+$ ILC3 (defined as Lin$^-$ RORγt-fm$^+$ NKp46$^+$ NK1.1$^+$) and NK/ILC1 (defined as Lin$^-$ RORγt-fm$^-$ NKp46$^+$ NK1.1$^+$) (Figure S5C) were isolated from eight week old Rorc(γt)-Cre^{Tg} × Rosa26R-YFP mice on a C57BL/6 background (H-2b), and were transferred intravenously into 8-week-old *Rag2*$^{-/-}$ *Il2rg*$^{-/-}$ mice, which were kept for 6 weeks under SPF conditions before analysis of RORγt expression in small and large intestine. Ex-RORγt$^+$ ILC3: N = 3; NK/ILC1: N = 2. Error bars (C) represent SEM.

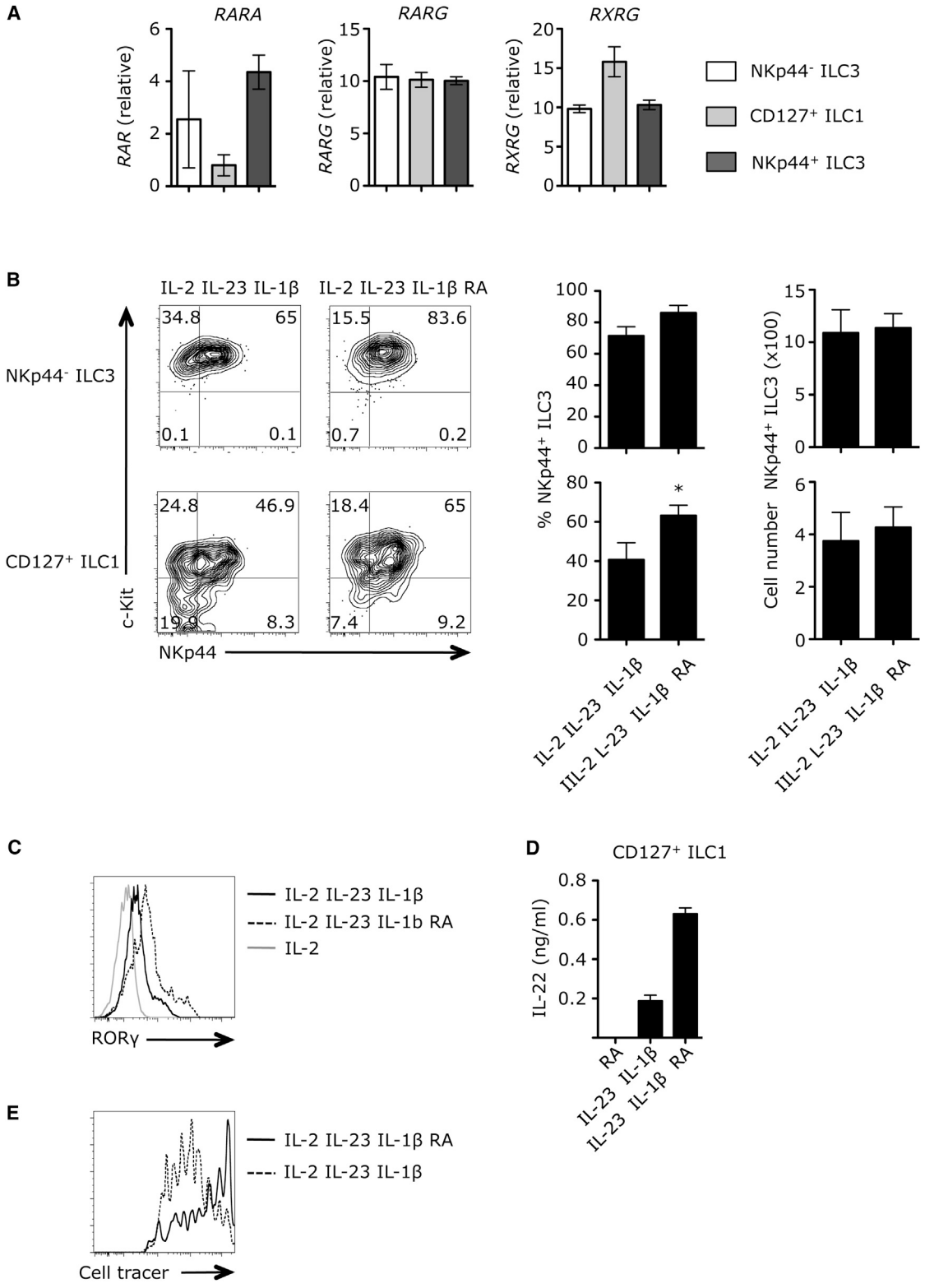

Figure 5. RA Accelerates ILC3 Differentiation and IL-22 Production

(A) Expression of *RARA*, *RARG*, and *RXRG* of CD127$^+$ ILC1 and ILC3 subsets, presented relative to the expression of *ACTB* (which encodes β-actin) of freshly isolated CD127$^+$ ILC1 NKp44$^-$ ILC3, and NKp44$^+$ ILC3. Data shown is combined data of at least 3 experiments with 1 to 2 donors each.

(B) Freshly isolated CD127$^+$ ILC1, and NKp44$^-$ ILC3, from tonsil are cultured for 4 days either with IL-2 IL-23, and IL-1β or with IL-2, IL-23, IL-1β, and retinoic acid (RA). Cells were phenotyped for the expression of c-Kit and NKp44 and numbers in quadrants indicate percent cells in each. Data shown is

(legend continued on next page)

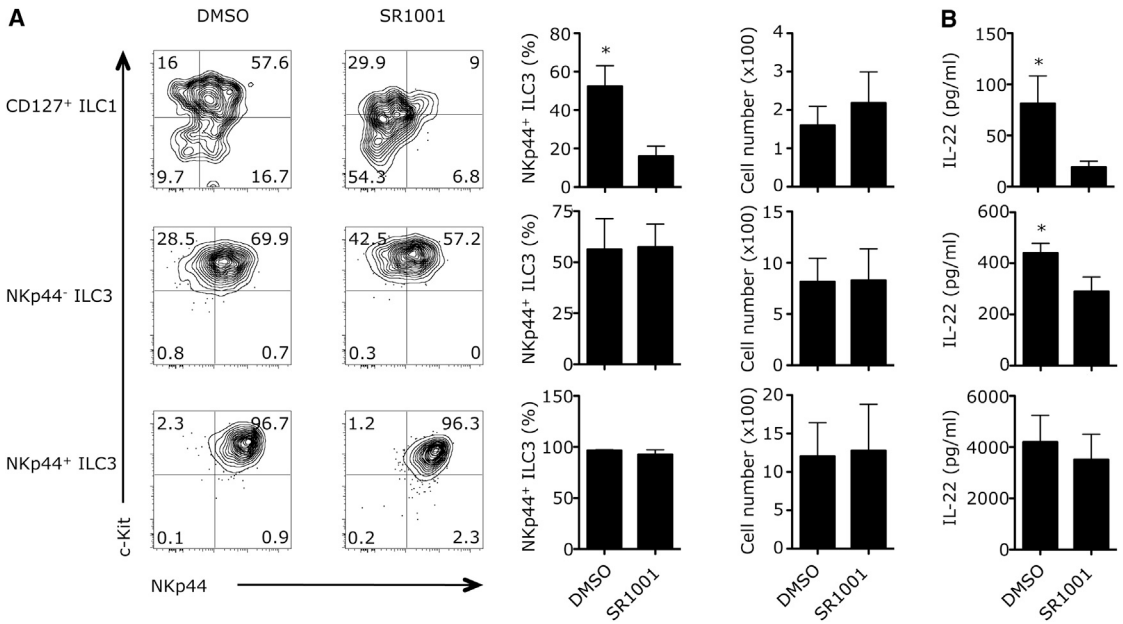

Figure 6. CD127⁺ ILC1 Derived Differentiation to ILC3 Is Controlled by RORγt

(A) Freshly isolated CD127⁺ ILC1, NKp44⁻ ILC3, and NKp44⁺ ILC3 from tonsil are cultured for 4 days with IL-2 IL-23, IL-1β, and RA in the presence of either SR1001 or DMSO. Cells are phenotyped for the expression of c-Kit and NKp44. Numbers in quadrants indicate percentage cells in each. On the right, bar diagrams indicate absolute cell number and percentage of c-Kit⁺ NKp44⁺ cells of each subset cultured in either SR1001 or DMSO.

(B) IL-22-production by CD127⁺ ILC1, NKp44⁻ ILC3, and NKp44⁺ ILC3, cultured as in 6a. Data shown is combined data of 3 experiments. *p < 0.05 (Mann-Whitney test). Error bars (A, B) represent SEM.

another research group identified human ILC subsets that shared the capacity to produce IFN-γ (Bernink et al., 2013; Fuchs et al., 2013). These subsets were distinct from each other; one expressed high amounts of CD127, whereas the other expressed the integrin CD103 and only low amounts of CD127. Here we compared these two subsets side by side. We confirmed that CD103⁺ ILC1 are located within the epithelium of the intestine, whereas CD127⁺ ILC1 reside in the lamina propria. Both populations were present only in very low numbers in fetal intestine, which suggests that colonization by microbiota may trigger their appearance in the intestine. We found that CD127⁺ and CD103⁺ ILC1 were equally distributed in both tonsil and non-inflamed intestinal resection specimen. In inflamed resection specimens of individuals with Crohn's disease, we observed a dramatic increase in frequency of CD127⁺ ILC1 whereas the proportions of CD103⁺ ILC1 also increased but to a substantially lesser extent.

In mice a distinct subset of ILC1 has been recently characterized which also lacked Eomes but were NKp46⁺ Tbet⁺ and RORγt-fm⁻, meaning that these cells never expressed RORγt during their development (Klose et al., 2014). This ILC1 subset was mainly present in the mucosal tissues, such as the intestine (Klose et al., 2014). Although the human CD127⁺ ILC1 subset described here also lack Eomes, they also lacked expression of the natural cytotoxicity receptors (NCRs) NKp46 and NKp44. CD103⁺ ILC1 have been described to express perforin and granzymes, and mostly co-express Eomes and Tbet, and therefore may represent a subset of cNK cells specifically located in the epithelium. Thus the human cell types described here are probably distinct from the mouse RORγt fate-map⁻ ILC1 and the human equivalent of these cells has yet to be indentified.

Previous studies in human and mouse systems have provided evidence that ILC3, particularly in the intestine, have the ability to upregulate T-bet and downregulate RORγt, both in vitro and in vivo (Bernink et al., 2013; Klose et al., 2013; Vonarbourg et al., 2010). Here we reported that human IFN-γ-producing CD127⁺ T-bet⁺ c-Kit⁻ NKp44⁻ ILC1 can differentiate into IL-22-producing NKp44⁺ ILC3. This differentiation was induced by IL1β and IL-23, coincided with increased levels of RORγt and decreased levels of T-bet and was amplified by RA. Since RA has been shown to directly upregulate RORγt (van de Pavert

representative of at least 4 independent experiments with 1 to 2 donors each. Percentage of c-Kit⁺ NKp44⁺ cells and cell numbers are indicated in bar diagrams on the right.

(C) Freshly isolated CD127⁺ ILC1 from tonsil are cultured for 7 days with either IL-2 (gray line), with IL-2, IL-23, and IL-1β (black line), or with IL-2, IL-23, IL-1β, and RA (dotted line), followed by intracellular staining for RORγt. Data shown is representative of 2 experiments with 2 donors each.

(D) Il-22 production by CD127⁺ ILC1, cultured for 4 days with RA alone, with IL-2, IL-23, and IL-1β, or IL-2, IL-23, IL-1β, and RA. Data shown is representative of 3 experiments with 1 donor each.

(E) Flow cytometry of CD127⁺ ILC1 stimulated for 7 days with either IL-2 IL-23 IL-1β (dotted line) or IL-2 IL-23 IL-1β, and RA (black line), which were stained with a proliferation dye. Data shown is representative of 5 experiments with 1 donor each. *p < 0.05 (Mann-Whitney test). Error bars (A, B, D) represent SEM.

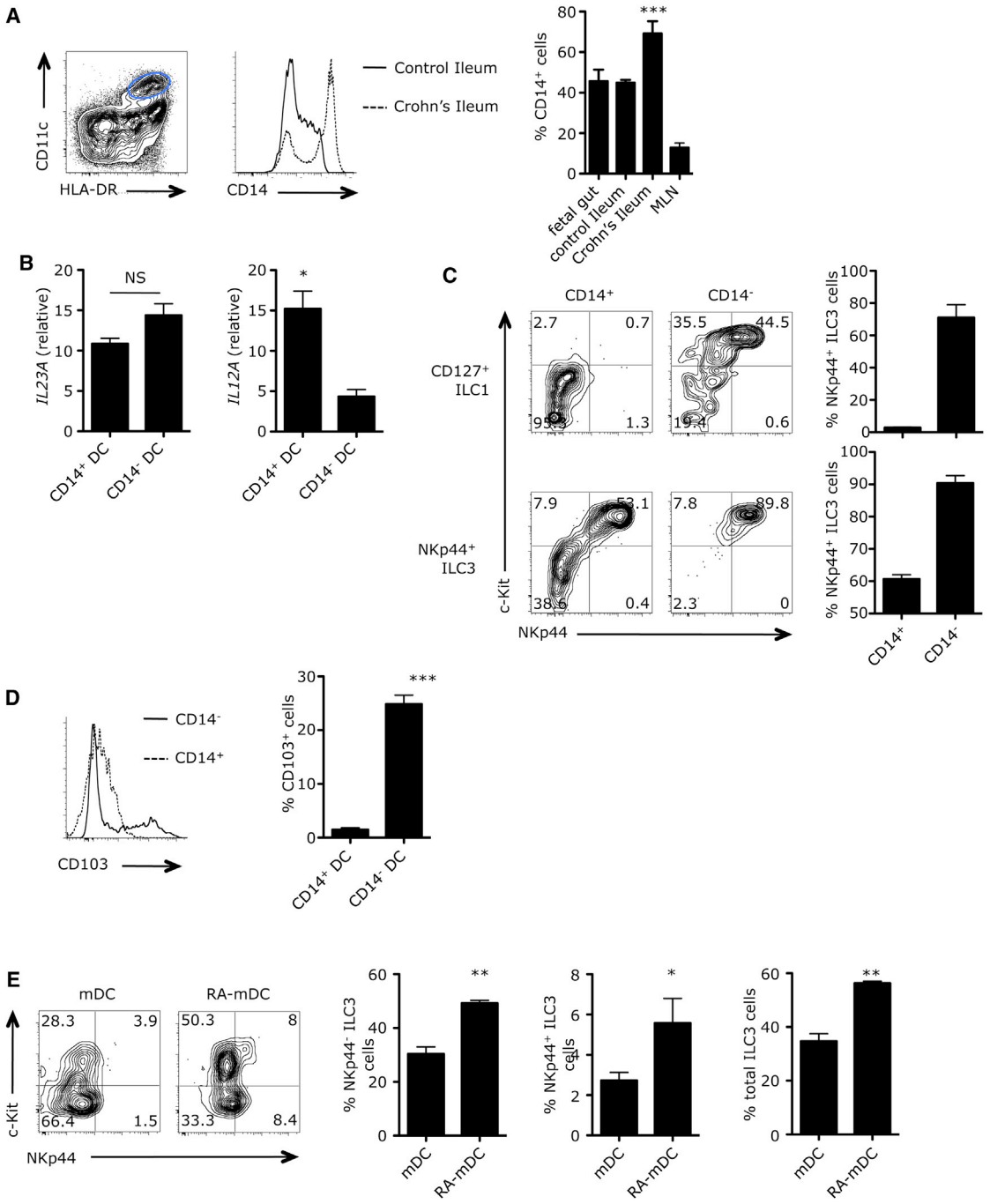

Figure 7. Intestinal Dendritic Cells (DCs) Control Differentiation of CD127$^+$ ILC1 toward ILC3

(A) Gating strategy of intestinal DCs. Cells were pre-gated on CD3$^-$, CD45$^+$ (data not shown), followed by gating on HLA-DR and CD11c. Fetal gut, non-inflamed ileal (control), and Crohn's disease ileal DCs, and MLN DCs were analyzed for the expression of CD14 and quantified in bar diagrams. ***$p < 0.001$ (analysis of variance).

(B) Expression of *IL23A* and *IL12A* in freshly isolated ileal CD14$^+$ and CD14$^-$ DC subsets, relative to the expression of *ACTB* (which encodes for β-actin). Data shown is combined data of 3 independent experiments with 1 donor each. *$p < 0.05$ (Mann-Whitney test).

(C) Autologous co-culture assay between either freshly isolated intestinal CD14$^-$ or CD14$^+$ DCs (isolated according to gating strategy in A) and CD127$^+$ ILC1 and ILC3 (isolated according to gating strategy in Figure 1A). Cells were cultured for 4 days. Numbers in quadrants indicate percentage cells in each. On the right, bar diagrams indicate percentage of c-Kit$^+$ NKp44$^+$ cells.

(D) CD103 expression on CD14$^+$ and CD14$^-$ intestinal DCs. On the right the bar diagram in which the percentage is quantified. ***$p < 0.001$ (Mann-Whitney test).

(E) In vitro generated mDC and RA-mDCs (as shown in methods) were stimulated with LPS and co-cultured with freshly isolated tonsil CD127$^+$ ILC1, NKp44$^-$ ILC3, NKp44$^+$ ILC3 for 4 days. Cells were analyzed for the expression of c-Kit and NKp44. Numbers in quadrants indicate percentage cells in each. Data shown is representative of at least 3 independent experiments. On the right the bar diagram in which the percentage is quantified. *$p < 0.05$ (Student's t test). Error bars (A–E) represent SEM.

et al., 2014), those findings raised the possibility of an involvement of RORγt in this process. This notion is reinforced by the finding that SR1001, an antagonist binding to the ligand binding domain of RORγt (Solt et al., 2011), inhibited ILC3 differentiation. Not only the frequency of NKp44$^+$ ILC3, but also the accumulation of IL-22 during the differentiation process was reduced by the RORγt inhibitor. Importantly, SR1001 did not inhibit IL-22 production by ex vivo isolated NKp44$^+$ ILC3, suggesting that the reduction of IL-22 production in the ILC1 differentiation cultures was the result of inhibition of the differentiation process of ILC1 into ILC3 and not of the effector function of ILC3 after completion of the differentiation process. However, it should be noted that not all CD127$^+$ ILC1 differentiated toward ILC3 in the presence of IL-2, IL-1β, and IL-23. Between 2%–15% of the cells kept their ILC1 phenotype. Whether these cells constitute a distinct subset or whether a certain equilibrium is maintained between the subsets remains an open question and needs to be further investigated.

Using HIS-mice, we previously observed that CD127$^+$ ILC1 expanded in frequency promptly upon inflammation in the gut (Bernink et al., 2013). We proposed that the accumulation of ILC1 under those conditions is the result of a rapid inflammation-induced differentiation of NKp44$^+$ ILC3, which dominate under homeostatic conditions, into ILC1. This conversion was dependent on IL-12 (Bernink et al., 2013; Vonarbourg et al., 2010). Gut inflammation triggers the influx of IL-12 producing phagocytes (Goldszmid et al., 2012; Neurath, 2014; Schulthess et al., 2012). In line with those findings we observed in intestinal resection specimen from people with Crohn's disease an elevated frequency of *IL12* expressing CD14$^+$ DCs compared to non-inflamed control, and ex vivo isolated CD14$^+$ DC cultures in the presence of NKp44$^+$ ILC3 were sufficient to drive ILC3 to ILC1 differentiation. CD14$^-$ DCs dominate under homeostatic conditions, and these cells were sufficient to drive ILC1 to ILC3 differentiation. Our observation that human ILC1 can also differentiate into ILC3 in reconstituted HIS mice and that mouse ILC3-derived ILC1 (or ex-ILC3) differentiate into ILC3 in lymphopenic mice, raises the possibility that after resolution of inflammation the "inflammatory" IFN-γ-producing CD127$^+$ ILC1 revert to "homeostatic" IL-22-producing ILC3. Further evaluation of the CD14$^-$ population revealed approximately 25% of these cells expressed CD103, which marks an RA-producing tissue resident DC population. Direct comparison of monocyte-derived DCs and RA-producing CD103$^+$ DCs (Bakdash et al., 2014) revealed that the latter were superior in driving ILC1 to ILC3 conversion compared to the mDCs. Thus, DCs respond differently to environmental cues, which enable them to instruct the ILCs.

Several studies in mice support the idea that DCs are important in instructing ILCs. In one study, it was demonstrated that basal production of Il-1β by a subset of gut-resident macrophages in mice was essential for ILC3 homeostasis locally and in MLN. Crosstalk between these macrophages and ILC3 instructed CD103$^+$ DCs to produce RA, which in turn contributed to intestinal homeostasis (Mortha et al., 2014). Another study demonstrated that CD103$^+$ DCs are a cellular source of IL-23, which have been demonstrated to interact and activate ILCs in a transient manner (Kinnebrew et al., 2012).

Our data suggest that RA is an important regulator of ILC1 to ILC3 conversion. RA is present in high concentrations in the gastrointestinal tract (Veldhoen and Brucklacher-Waldert, 2012). Epithelial-derived RA has been shown to influence processes of immune cells located in the lamina propria. For example, RA drives differentiation of monocytes toward CD103$^+$ DCs, which acquired a tolerogenic phenotype and thereby able to drive regulatory T cell differentiation (Iliev et al., 2009). RA also has a direct effect on mouse ILC3 by promoting the upregulation of IL-22 (Mielke et al., 2013), and in another study it was demonstrated that the gut-resident ILC composition is directly influenced by RA, favoring ILC3 over ILC2 (Spencer et al., 2014). In line with these reports, we observed in our in vitro cultures that RA, in combination with IL-2, IL-23, and IL-1β, induced human ILC3 differentiation and enhanced IL-22 production. This, together with the notion that high titers of RA are readily produced by epithelial cells and lamina propria-resident CD103$^+$ DCs, may explain our observation that adult gut-resident CD127$^+$ ILCs predominantly comprised the NKp44$^+$ ILC3 compartment and lacked CRTH2$^+$ ILC2. These NCR$^+$ ILC3 expressed high levels of *IL22* under homeostatic conditions compared to NKp44$^-$ ILC3 and ILC1, possibly in order to maintain the integrity of the epithelial barrier during homeostasis (Sonnenberg and Artis, 2012).

We found in intestinal resection specimen of Crohn's disease patients an increased frequency of IFN-γ producing CD127$^+$ ILC1, which was inversely proportional to the reduced frequency of NKp44$^+$ ILC3. Intestinal inflammation, such as Crohn's disease, is accompanied by an influx of pro-inflammatory IL-12 producing phagocytes at the site of infection (Goldszmid et al., 2012), which may drive the differentiation of ILC3 toward CD127$^+$ ILC1. IFN-γ in turn, has been reported to orchestrate the replacement of resident mononuclear phagocytes by circulating pro-inflammatory monocytes (Goldszmid et al., 2012), reinforcing the pro-inflammatory milieu at the site of infection. Furthermore, it was reported that IFN-γ signals directly on Paneth cells in the intestinal crypts, instructing them to release antimicrobial compounds, which was coupled to the extrusion and death of Paneth cells (Farin et al., 2014). Concordantly, prolonged IFN-γ responses do harm the host, resulting in severe gut inflammation (Buonocore et al., 2010; Klose et al., 2014; Vonarbourg et al., 2010). Therefore, it is tempting to speculate that persistently increased numbers of ILC1 contribute to the disease process. If this is the cas,e it might be possible that enforcing differentiation of these ILC1 to ILC3 may have a therapeutic effect in Crohn's disease. In this respect, it is noteworthy that ILC1 isolated from surgical specimens of Crohn's disease patients also convert to NKp44$^+$ ILC3.

Taken together, an efficient mechanism presents itself by which ILC can quickly adapt to changes inflicted by pathogens without the need of recruiting new cells from the circulation. Furthermore, the identification of environmental cues and transcription factors that drive this plasticity may be used to develop future targets for potential therapeutic interventions.

EXPERIMENTAL PROCEDURES

Tissue Collection

All tissues were collected after subjects provided informed consent, with approval of tissue-specific protocols by the Medical Ethical Committee of the Academic Medical Centre, Amsterdam. Tonsils were obtained from

pediatric tonsillectomies. Inflamed intestinal ileum of patients with Crohn's disease was freshly obtained and processed after surgical resection. Non-inflamed ileum, referred to as "non-inflamed control," was collected after surgical resection of colon cancer, where the ileum was considered unaffected. Subjects were excluded if they had undergone chemo- or radiotherapy before resection. Patients' age range is from 18 to 68 years. Human fetal tissues were obtained from elective abortions at the Stichting Bloemenhove clinic in Heemstede, the Netherlands, upon on the receipt of informed consent. The use of human abortion tissues was approved by the Medical Ethical Committee of the Academic Medical Center, Amsterdam. Gestational age, determined by ultrasonic measurement of the diameter of the skull or femur, ranged from 14 to 17 weeks.

Human Immune System Mice

$CD34^+$ $CD38^-$ HSCs isolated from human fetal liver ($0.2 \times 10^5 - 2 \times 10^5$ cells) were transplanted intrahepatically into sublethally irradiated (1.0 Gy) newborn NSG mice (younger than 1 week of age). Peripheral blood was collected from a facial vein every 3 to 4 weeks after transplantation to determine the kinetics of human cell engraftment. At 2 months of age, mice were retro-orbital inoculated with approximately $1 \times 10^5 - 5 \times 10^5$ expanded and cell tracker labeled $CD127^+$ ILC1 (as described in Bernink et al.). After 4 days, mice were sacrificed and organs were harvested for analyses.

Transfer Experiments

ILC populations were prepared from 8-week-old Rorc(γt)-Cre^{Tg} x Rosa26R-YFP mice on a C57BL/6 background (H-2b) (as described in Vonarbourg et al., 2010). Ex-$ROR\gamma t^+$ ILC3 were defined as Lin^- $ROR\gamma t\text{-}fm^+$ $NKp46^+$ $NK1.1^+$ cells and the NK/ILC1 population was defined as Lin^- $ROR\gamma t\text{-}fm^-$ $NKp46^+$ $NK1.1^+$ cells. Using a BD FACS Aria III cell sorter, cells were sorted into Eppendorf tubes filled with 500 μl Dulbecco's Modified Eagle Medium (DMEM) supplemented with 10% FCS, 10mM HEPES, 1mM Sodium Pyruvate plus nonessential amino acids, 80 mM 2-Mercaptoethanol, 8 mg/ml Glutamine, 100 U/ml Penicillin, 0.4 mg/ml Gentamicin, and 100 mg/ml Streptomycin. Cells were subsequently washed in PBS and 8,000 cells were transferred intravenously into 8-week-old *Rag2*$^{-/-}$ *Il2rg*$^{-/-}$ mice. Mice were kept for 6 weeks under SPF conditions at which time they were analyzed.

Isolation of Cells

Tonsil tissue was cut in small pieces and mechanically disrupted using the Stomacher 80 Biomaster (Seward). Cell suspension was passed through a 70 μm cell strainer and mononuclear cells were isolated with Ficoll-Paque Plus medium (GE Healthcare).

Intestinal lamina propria was incubated for 30 min with PBS containing 5 mM EDTA at 37°C to separate epithelial cells from lamina propria cells. Lamina propria was then cut into small pieces and digested for 30 min at 37°C with RPMI (GIBCO) containing Liberase TM (125 μg/ml). Cell suspensions were filtered through a 70 μm nylon mesh, and intraepithelial and lamina propria mononuclear cells were isolated with Ficoll-Paque Plus medium (GE Healthcare). In some experiments IEL and LP fractions were analyzed separately, and in some experiments both fractions were combined before analysis. Mesenteric lymph nodes were mechanically disrupted and were passed through a 70 μm cell strainer and mononuclear cells were isolated with Ficoll-Paque Plus medium.

Isolation of lamina propria lymphocytes (LPL) in mice was performed as described in Sanos and Diefenbach (2010). In short: small intestines were removed, Peyer's patches were excised, and the intestines were flushed with ice-cold PBS and cut longitudinally. Epithelium was dissociated by incubation for 40 min at 37°C in Hank's Balanced Salt Solution without Ca^{2+}/Mg^{2+} (HBSS) with 5 mM EDTA and 10 mM HEPES and subsequent vortexing. Remaining tissue, containing LPL, was minced with a scalpel and digested in HBSS (with Ca^{2+}/Mg^{2+}) containing Collagenase D (0.5 mg/ml), DNase I (0.5 mg/ml), and Dispase (0.5 U/ml) for 1 hr at 37°C under constant shaking. Cells were detached by thorough vortexing and filtered through a 70 μM filter. Leukocytes were enriched using a Percoll Gradient centrifugation. Cells were resuspended in PBS containing 2% FCS and stained for 30 min on ice with fluorochrome-conjugated antibodies.

Flow Cytometry Analysis and Sorting

The antibodies used to human and mice proteins are listed in Table S3. For phenotypic analyses by flow cytometry, data were collected with an LSR-Fortessa instrument (BD Biosciences). For sorting by flow cytometry an ARIA IIU (BD Biosciences) was used. Data was analyzed with FlowJo software (TreeStar). Peripheral blood and tonsil mononuclear cell samples were depleted of T cells and B cells by labeling with FITC-conjugated anti-CD3 and anti-CD19 (described above) plus anti-FITC microbeads (Miltenyi).

Intracellular Cytokine Staining

Cell cultures were stimulated for 6 hr with PMA (10 ng/ml; Sigma) and ionomycin (500 nM; Merck) in the presence of GolgiPlug (BD Biosciences) for the final 4 hr of culture. A Cytofix/Cytoperm kit (BD Biosciences) was used for cell permeabilization, staining, and subsequent washing. The following antibodies were used: allophycocy- anin-conjugated IL-17 (BL168; BioLegend), and phycoerythrin-conjugated anti-IL-22 (142928; R&D Systems) and anti-IFN-γ-pe-cy7 (B27; BD Bioscience). Data were acquired with an LSRFortessa instrument (BD Biosciences) and analyzed with FlowJo software (TreeStar).

Quantative Real-Time PCR

RNA was isolated with NucleoSpin RNA XS kit (Macherey-Nagel) according to the manufacturer's protocol. Complementary DNA was synthesized with the High-Capacity cDNA Archive kit (Applied Biosystems). PCR was done on a LightCycler 480 Instrument II (Roche) with SYBR Green I master mix (Roche). Primers sets used are shown in Table S2.

Cell Cultures and RORγt Inhibition

For short-term cultures (2 to 7 days), $CD103^+$ ILC1, cNK cells, and Lin^- $CD127^+$ ILC populations were cultured in some experiments with or in some experiments without irradiated allogeneic peripheral blood mononuclear cells (25 Gy), irradiated Epstein-Barr virus–transformed JY human B cells (50 Gy), phytohemagglutinin (1 μg/ml; Oxoid), and IL-2 (100 U/ml; Novartis) in Yssel's medium (AMC; made in house) supplemented with 1% (vol/vol) human AB serum. For ILC3 polarization experiments IL-23 (50 ng/ml; R&D Systems), and IL-1β (50 ng/ml; R&D Systems), and in indicated experiments retinoic acid (RA) (1 μM; Sigma-Aldrich) were supplemented to cultures. For ILC1 polarizing experiments IL-12 (50 ng/ml; R&D Systems) was supplemented to cultures. Inhibition of RORγt was achieved by the addition of the synthetic RORγt-ligand SR1001 (10 μM; Sigma-Aldrich) to cell cultures with freshly isolated $CD127^+$ ILC1 and ILC3, which were cultured in the presence of IL-2 (10 U/ml; Novartis) IL-23 (50 ng/ml; R&D Systems), and IL-1β (50 ng/ml; R&D Systems and RA (1 μM; Sigma-Aldrich) and RA (1 μM; Sigma-Aldrich).

Generation of mDC and RA-mDC

RA-mDCs and mDCs were generated as described in (Bakdash et al., 2014). In brief, monocytes were isolated from PBMCs using density centrifugation, then cultured for 6 days in IMDM (GIBCO) containing gentamicin (86 μg/l; Duchefa) and 10% FCS (GIBCO), supplemented with GM-CSF (500 U/ml; Schering-Plough) and IL-4 (10 IU/ml; Miltenyi Biotech, Bergisch Gladbach, Germany). RA-DCs were generated in the additional presence of 1 μM of retinoic acid (Sigma-Aldrich).

Aldefluor Assay

The ALDH activity of DCs was determined by the ALDEFLUOR staining kit (Aldagen) following manufacturer's instructions.

Cytokine Production

Freshly isolated $CD103^+$ ILC1, $CD127^+$ ILC1, and cNK cells (2,000 cells per well in a 96-well plate) were stimulated for 4 days with combinations of IL-2 (10 U/ml; Novartis), IL-12 (50 ng/ml; R&D Systems), IL-18 (50 ng/ml; R&D Systems), IL-15 (50 ng/ml; R&D Systems). Cytokine production was measured by enzyme-linked immunosorbent assay (ELISA). IFN-γ (eBioscience) and IL-22 (R&D) were measured from supernatants of cultures.

Statistical Analysis

Statistical significance was determined with ANOVA, Student's t test, or Mann-Whitney test. Prism GraphPad software was used.

SUPPLEMENTAL INFORMATION

Supplemental Information includes seven figures and three tables and can be found with this article online at http://dx.doi.org/10.1016/j.immuni.2015.06.019.

ACKNOWLEDGMENTS

We thank B. Hooibrink for help with flow cytometry; staff of the Bloemenhove clinic in Heemstede, the Netherlands, for fetal tissues; and K. Weijer for processing fetal material. H.S. is supported by an advanced grant of the European Research Council.

Received: August 29, 2014
Revised: February 27, 2015
Accepted: April 22, 2015
Published: July 14, 2015

REFERENCES

Artis, D., and Spits, H. (2015). The biology of innate lymphoid cells. Nature *517*, 293–301.

Bakdash, G., Vogelpoel, L.T., van Capel, T.M., Kapsenberg, M.L., and de Jong, E.C. (2014). Retinoic acid primes human dendritic cells to induce gut-homing, IL-10-producing regulatory T cells. Mucosal Immunol. *8*, 265–278.

Bernink, J.H., Peters, C.P., Munneke, M., te Velde, A.A., Meijer, S.L., Weijer, K., Hreggvidsdottir, H.S., Heinsbroek, S.E., Legrand, N., Buskens, C.J., et al. (2013). Human type 1 innate lymphoid cells accumulate in inflamed mucosal tissues. Nat. Immunol. *14*, 221–229.

Buonocore, S., Ahern, P.P., Uhlig, H.H., Ivanov, I.I., Littman, D.R., Maloy, K.J., and Powrie, F. (2010). Innate lymphoid cells drive interleukin-23-dependent innate intestinal pathology. Nature *464*, 1371–1375.

Cella, M., Fuchs, A., Vermi, W., Facchetti, F., Otero, K., Lennerz, J.K., Doherty, J.M., Mills, J.C., and Colonna, M. (2009). A human natural killer cell subset provides an innate source of IL-22 for mucosal immunity. Nature *457*, 722–725.

Cella, M., Otero, K., and Colonna, M. (2010). Expansion of human NK-22 cells with IL-7, IL-2, and IL-1beta reveals intrinsic functional plasticity. Proc. Natl. Acad. Sci. USA *107*, 10961–10966.

Coombes, J.L., Siddiqui, K.R., Arancibia-Cárcamo, C.V., Hall, J., Sun, C.M., Belkaid, Y., and Powrie, F. (2007). A functionally specialized population of mucosal CD103+ DCs induces Foxp3+ regulatory T cells via a TGF-beta and retinoic acid-dependent mechanism. J. Exp. Med. *204*, 1757–1764.

Crellin, N.K., Trifari, S., Kaplan, C.D., Satoh-Takayama, N., Di Santo, J.P., and Spits, H. (2010). Regulation of cytokine secretion in human CD127(+) LTi-like innate lymphoid cells by Toll-like receptor 2. Immunity *33*, 752–764.

Daussy, C., Faure, F., Mayol, K., Viel, S., Gasteiger, G., Charrier, E., Bienvenu, J., Henry, T., Debien, E., Hasan, U.A., et al. (2014). T-bet and Eomes instruct the development of two distinct natural killer cell lineages in the liver and in the bone marrow. J. Exp. Med. *211*, 563–577.

Farin, H.F., Karthaus, W.R., Kujala, P., Rakhshandehroo, M., Schwank, G., Vries, R.G., Kalkhoven, E., Nieuwenhuis, E.E., and Clevers, H. (2014). Paneth cell extrusion and release of antimicrobial products is directly controlled by immune cell-derived IFN-γ. J. Exp. Med. *211*, 1393–1405.

Fuchs, A., Vermi, W., Lee, J.S., Lonardi, S., Gilfillan, S., Newberry, R.D., Cella, M., and Colonna, M. (2013). Intraepithelial type 1 innate lymphoid cells are a unique subset of IL-12- and IL-15-responsive IFN-γ-producing cells. Immunity *38*, 769–781.

Goldszmid, R.S., Caspar, P., Rivollier, A., White, S., Dzutsev, A., Hieny, S., Kelsall, B., Trinchieri, G., and Sher, A. (2012). NK cell-derived interferon-γ orchestrates cellular dynamics and the differentiation of monocytes into dendritic cells at the site of infection. Immunity *36*, 1047–1059.

Gordon, S.M., Chaix, J., Rupp, L.J., Wu, J., Madera, S., Sun, J.C., Lindsten, T., and Reiner, S.L. (2012). The transcription factors T-bet and Eomes control key checkpoints of natural killer cell maturation. Immunity *36*, 55–67.

Iliev, I.D., Spadoni, I., Mileti, E., Matteoli, G., Sonzogni, A., Sampietro, G.M., Foschi, D., Caprioli, F., Viale, G., and Rescigno, M. (2009). Human intestinal epithelial cells promote the differentiation of tolerogenic dendritic cells. Gut *58*, 1481–1489.

Ivanov, I.I., McKenzie, B.S., Zhou, L., Tadokoro, C.E., Lepelley, A., Lafaille, J.J., Cua, D.J., and Littman, D.R. (2006). The orphan nuclear receptor RORgammat directs the differentiation program of proinflammatory IL-17+ T helper cells. Cell *126*, 1121–1133.

Kinnebrew, M.A., Buffie, C.G., Diehl, G.E., Zenewicz, L.A., Leiner, I., Hohl, T.M., Flavell, R.A., Littman, D.R., and Pamer, E.G. (2012). Interleukin 23 production by intestinal CD103(+)CD11b(+) dendritic cells in response to bacterial flagellin enhances mucosal innate immune defense. Immunity *36*, 276–287.

Klose, C.S., Kiss, E.A., Schwierzeck, V., Ebert, K., Hoyler, T., d'Hargues, Y., Göppert, N., Croxford, A.L., Waisman, A., Tanriver, Y., and Diefenbach, A. (2013). A T-bet gradient controls the fate and function of CCR6-RORγt+ innate lymphoid cells. Nature *494*, 261–265.

Klose, C.S., Flach, M., Möhle, L., Rogell, L., Hoyler, T., Ebert, K., Fabiunke, C., Pfeifer, D., Sexl, V., Fonseca-Pereira, D., et al. (2014). Differentiation of type 1 ILCs from a common progenitor to all helper-like innate lymphoid cell lineages. Cell *157*, 340–356.

Lazarevic, V., Chen, X., Shim, J.H., Hwang, E.S., Jang, E., Bolm, A.N., Oukka, M., Kuchroo, V.K., and Glimcher, L.H. (2011). T-bet represses T(H)17 differentiation by preventing Runx1-mediated activation of the gene encoding RORγt. Nat. Immunol. *12*, 96–104.

Mielke, L.A., Jones, S.A., Raverdeau, M., Higgs, R., Stefanska, A., Groom, J.R., Misiak, A., Dungan, L.S., Sutton, C.E., Streubel, G., et al. (2013). Retinoic acid expression associates with enhanced IL-22 production by γδ T cells and innate lymphoid cells and attenuation of intestinal inflammation. J. Exp. Med. *210*, 1117–1124.

Mortha, A., Chudnovskiy, A., Hashimoto, D., Bogunovic, M., Spencer, S.P., Belkaid, Y., and Merad, M. (2014). Microbiota-dependent crosstalk between macrophages and ILC3 promotes intestinal homeostasis. Science *343*, 1249288.

Neurath, M.F. (2014). Cytokines in inflammatory bowel disease. Nat. Rev. Immunol. *14*, 329–342.

Powell, N., Walker, A.W., Stolarczyk, E., Canavan, J.B., Gökmen, M.R., Marks, E., Jackson, I., Hashim, A., Curtis, M.A., Jenner, R.G., et al. (2012). The transcription factor T-bet regulates intestinal inflammation mediated by interleukin-7 receptor+ innate lymphoid cells. Immunity *37*, 674–684.

Sanders, T.J., McCarthy, N.E., Giles, E.M., Davidson, K.L., Haltalli, M.L., Hazell, S., Lindsay, J.O., and Stagg, A.J. (2014). Increased production of retinoic acid by intestinal macrophages contributes to their inflammatory phenotype in patients with Crohn's disease. Gastroenterology *146*, 1278–1288, e1271-1272.

Sanos, S.L., and Diefenbach, A. (2010). Isolation of NK cells and NK-like cells from the intestinal lamina propria. Methods Mol. Biol. *612*, 505–517.

Satoh-Takayama, N., Vosshenrich, C.A., Lesjean-Pottier, S., Sawa, S., Lochner, M., Rattis, F., Mention, J.J., Thiam, K., Cerf-Bensussan, N., Mandelboim, O., et al. (2008). Microbial flora drives interleukin 22 production in intestinal NKp46+ cells that provide innate mucosal immune defense. Immunity *29*, 958–970.

Schulthess, J., Meresse, B., Ramiro-Puig, E., Montcuquet, N., Darche, S., Bègue, B., Ruemmele, F., Combadière, C., Di Santo, J.P., Buzoni-Gatel, D., and Cerf-Bensussan, N. (2012). Interleukin-15-dependent NKp46+ innate lymphoid cells control intestinal inflammation by recruiting inflammatory monocytes. Immunity *37*, 108–121.

Solt, L.A., Kumar, N., Nuhant, P., Wang, Y., Lauer, J.L., Liu, J., Istrate, M.A., Kamenecka, T.M., Roush, W.R., Vidović, D., et al. (2011). Suppression of TH17 differentiation and autoimmunity by a synthetic ROR ligand. Nature *472*, 491–494.

Sonnenberg, G.F., and Artis, D. (2012). Innate lymphoid cell interactions with microbiota: implications for intestinal health and disease. Immunity *37*, 601–610.

Sonnenberg, G.F., Monticelli, L.A., Elloso, M.M., Fouser, L.A., and Artis, D. (2011). CD4(+) lymphoid tissue-inducer cells promote innate immunity in the gut. Immunity *34*, 122–134.

Sonnenberg, G.F., Monticelli, L.A., Alenghat, T., Fung, T.C., Hutnick, N.A., Kunisawa, J., Shibata, N., Grunberg, S., Sinha, R., Zahm, A.M., et al. (2012). Innate lymphoid cells promote anatomical containment of lymphoid-resident commensal bacteria. Science *336*, 1321–1325.

Spencer, S.P., Wilhelm, C., Yang, Q., Hall, J.A., Bouladoux, N., Boyd, A., Nutman, T.B., Urban, J.F., Jr., Wang, J., Ramalingam, T.R., et al. (2014). Adaptation of innate lymphoid cells to a micronutrient deficiency promotes type 2 barrier immunity. Science *343*, 432–437.

Spits, H., and Cupedo, T. (2012). Innate lymphoid cells: emerging insights in development, lineage relationships, and function. Annu. Rev. Immunol. *30*, 647–675.

Spits, H., Artis, D., Colonna, M., Diefenbach, A., Di Santo, J.P., Eberl, G., Koyasu, S., Locksley, R., McKenzie, A.N., Mebius, R.E., et al. (2012). Innate Lymphoid Cells – a proposal for a uniform nomenclature. Nat. Immunol. Rev. *13*, 145–149.

van de Pavert, S.A., and Mebius, R.E. (2010). New insights into the development of lymphoid tissues. Nat. Rev. Immunol. *10*, 664–674.

van de Pavert, S.A., Ferreira, M., Domingues, R.G., Ribeiro, H., Molenaar, R., Moreira-Santos, L., Almeida, F.F., Ibiza, S., Barbosa, I., Goverse, G., et al. (2014). Maternal retinoids control type 3 innate lymphoid cells and set the offspring immunity. Nature *508*, 123–127.

Veldhoen, M., and Brucklacher-Waldert, V. (2012). Dietary influences on intestinal immunity. Nat. Rev. Immunol. *12*, 696–708.

Vonarbourg, C., Mortha, A., Bui, V.L., Hernandez, P.P., Kiss, E.A., Hoyler, T., Flach, M., Bengsch, B., Thimme, R., Hölscher, C., et al. (2010). Regulated expression of nuclear receptor RORγt confers distinct functional fates to NK cell receptor-expressing RORγt(+) innate lymphocytes. Immunity *33*, 736–751.